Supporting Information

Engineering Electron-Deficiency and Wettability of Cu-based Catalysts using Arylamine Ligands to Promote Electrocatalytic Oxygen Reduction

Kaiyuan Wang,†[a] Yuan Xu,†[a] Fei He,[b] Yanqin Lv,*[c] Yanfei Shen,*[d] Songqin Liu,[a] Yuanjian Zhang*[a]

[a]*Jiangsu Engineering Research Center for Carbon-Rich Materials and Devices, Jiangsu Province Hi-Tech Key Laboratory for Bio-Medical Research, School of Chemistry and Chemical Engineering, Southeast University, Nanjing 211189, China. E-mail: Yuanjian.Zhang@seu.edu.cn*
[b]*School of Material Science and Engineering, University of Jinan, Jinan 250022, China.*
[c]*College of Chemistry, Chemical Engineering and Materials Science, Shandong Normal University, Jinan 250014, China. E-mail: yanqinlv@sdnu.edu.cn*
[d]*Medical School, Southeast University, Nanjing 210009, China. E-mail: Yanfei.Shen@seu.edu.cn*

† These authors contributed equally to this work.

Experimental section

Chemicals. Copper (II) sulfate pentahydrate ($CuSO_4 \cdot 5H_2O$), ammonia, acetone, potassium hydroxide (KOH), methanol, and ethylenediaminetetraacetic acid sodium (EDTA) were purchased from Sinopharm Chemical Reagent Co., Ltd. (China). HRP and 20% Pt/C were purchased from Sigma-Aldrich. 3,3'-diaminobenzidine tetrahydrochloride (DAB·4HCl), 1,2,4,5-benzenetetramine tetrahydrochloride (BTA·4HCl), and 4,6-diaminoresorcinol dihydrochloride (DAR·2HCl) were purchased from Shanghai Macklin Biochemical Co., Ltd. (China). Ketjenblack EC600J carbon black (CB) was purchased from AkzoNobel N.V. (Netherlands). All other chemicals were used without further purification, unless otherwise specified. Ultrapure water (18.2 MΩ cm) used in all experiments was obtained from a Direct-Q 3 UV pure water purification system (Millipore, USA).

Characterization. Elemental analysis was performed using a Vario EL III analyzer (Germany). Inductively coupled plasma mass spectrometry (ICP-MS) was performed using an Agilent 7900 instrument (USA). Electron paramagnetic resonance (EPR) spectroscopy was performed using a Bruker A300-10-12 spectrometer (Germany) with a 100 kHz modulation frequency at room temperature. Scanning electron microscopy (SEM) images were obtained using a Navo Nano SEM450 scanning electron microscope (America). Transmission electron microscopy (TEM) images were obtained using a Talos F200X transmission electron microscope (USA). X-Ray Photoelectron Spectroscopy (XPS) experiments were performed using a Thermo Theta probe (USA) with monochromated Al Kα X-rays at hν 1486.6 eV. The peak positions were internally referenced to the C1s peak at 284.6 eV. UV-vis absorption spectroscopy was performed using an Agilent Cary 10 UV-Vis spectrophotometer (USA). Fourier transform infrared (FT-IR) spectroscopy was performed using a Thermo Nicolet iS10 FT-IR spectrometer (USA). Electrochemical measurements were performed using a CHI760E workstation (USA) and RRDE-3A rotating ring-disk electrodes (ALS, Japan).

Preparation of Cu-based catalysts

Cu-BTA/C: Cu-BTA/C was prepared according to a previously reported method. Typically, 3,3'-diaminobenzidine tetrahydrochloride (DAB·4HCl, 1 mmol) in distilled

water (100 mL) was stirred in a round-bottom flask at RT under air. Then, Ketjenblack EC600J CB (330 mg) was added and ultrasonically dispersed in the solution. Subsequently, a solution of $CuSO_4$ (1 mmol) in distilled water (70 mL) and concentrated aqueous ammonia (28 wt%, 3.5 mL) was added and stirred for 3 h. The mixture was centrifuged, rinsed with distilled water and acetone successively, and dried under vacuum at 60 ºC to yield Cu-DAB/C.

Cu-DAB/C: Cu-DAB/C was prepared according to the reported method. Typically, 1,2,4,5-benzenetetramine tetrahydrochloride (BTA·4HCl, 1 mmol) was stirred in distilled water (100 mL) in a round-bottom flask at RT under air. Then, Ketjenblack EC600J CB (330 mg) was added and ultrasonically dispersed in the solution. After that, a solution of $CuSO_4$ (1 mmol) in distilled water (70 mL) and concentrated aqueous ammonia (28 wt%, 3.5 mL) was added and stirred for 3 h. The mixture was centrifuged, rinsed with distilled water and acetone successively, and dried under vacuum at 60 ºC to yield Cu-BTA/C.

Cu-DAR/C: Cu-DAB/C was prepared according to the reported method. Typically, 4,6-diaminoresorcinol dihydrochloride (DAR·2HCl, 1 mmol) in distilled water (100 mL) was stirred in a round-bottom flask at RT under air. Then, Ketjenblack EC600J CB (330 mg) was added and ultrasonically dispersed in the solution. After that, a solution of $CuSO_4$ (1 mmol) in distilled water (70 mL) and concentrated aqueous ammonia (28 wt%, 3.5 mL) was added and stirred for 3 h. The mixture was centrifuged, rinsed with distilled water and acetone successively, and dried under vacuum at 60 ºC to yield Cu-BTA/C.

Electrochemical measurements. The ORR activities of Cu-BTA/C, Cu-DAB/C, Cu-DAR/C, and 20% Pt/C were measured in a standard three-electrode glass cell on a CHI760E workstation (CHI, USA). A rotating disk electrode (RDE) or rotating ring-disk electrode (RRDE) modified with an electrocatalyst was used as the working electrode. A Pt wire and Ag/AgCl (saturated KCl) were used as the counter and reference electrodes, respectively. A 0.1 M KOH aqueous solution was chosen as the electrolyte during the electrochemical investigation. The working electrode was modified as described below. 7 μL of the electrocatalysts dispersion in ethanol (4 mg mL^{-1}) was cast on the pre-polished surface of a RDE (3 mm diameter) or RRDE (4

mm diameter), resulting in a catalyst loading of 397 μg cm^{-2}. Subsequently, 5 μL of Nafion (0.05 wt. %) was further cast on the surface of the electrode.

For the ORR test, 0.1 M KOH was saturated with high-purity O_2. Thereafter, the electrolyte was protected by O_2 flow. The ORR activity was measured using linear sweep voltammetry (LSV) with a rotating electrode system (RRDE-3A, BAS, Japan). LSV was recorded at a scan rate of 10 mV s^{-1}. The reversible hydrogen electrode (RHE) was calculated using the equation E(RHE)=0.196+ E(Ag/AgCl)+0.0592×pH. The charging current was recorded at the same scan rate in N_2-saturated 0.1 M KOH solution. In this study, the onset potential (E_{onset}) is defined as the potential at which the current density reaches 5% of the diffusion-limiting current density in the cathodic scan. The half-wave potential ($E_{1/2}$) is defined as the potential at which the current density reaches 50% of the diffusion-limiting current density in the cathodic scan.

The kinetic current (J_k) for the ORR can be derived from the experimental data using the Koutecky-Levich equation for rotating disk electrodes:

$$\frac{1}{J} = \frac{1}{J_K} + \frac{1}{J_L} = \frac{1}{J_K} + \frac{1}{B\omega^{1/2}} \quad (1)$$

$$B = 0.62nFC_0(D_0)^{\frac{2}{3}}\nu^{-\frac{1}{6}} \quad (2)$$

$$J_K = nFkC_0 \quad (3)$$

in which J is the measured current density, J_K and J_L are the kinetic- and diffusion-limiting current densities, ω is the angular velocity of the rotating electrode ($\omega = 2\pi N$, N is the linear rotation speed), n is the exchange electron transfer number in ORR, F is the Faraday constant (F=96485 C mol^{-1}), C_0 is the concentration of O_2, D_0 is the diffusion coefficient of O_2, ν is the kinematic viscosity of the electrolyte, and k is the electron transfer rate constant. Since the electrolyte was O_2 saturated 0.1 M KOH in this report, C_0, D_0 and ν were used as 1.2×10^{-3} M, 1.9×10^{-5} cm^2 s^{-1}, and 0.01 cm^2 s^{-1}, respectively.

To detect the H_2O_2 yield, the ring potential was set to 0.5 V vs. Ag/AgCl to oxidize the H_2O_2 transferred from the GC disk electrode. The H_2O_2 yield and electron transfer number (n) were calculated using the following equation:

$$H_2O_2\ (\%) = 200 \times \frac{I_R/N_0}{(I_R/N_0)+I_D} \quad (4)$$

$$n = 4 \times \frac{I_D}{(I_R/N_0)+I_D} \quad (5)$$

Where I_D and I_R are the disk and ring currents, respectively, and N_0 is the ring collection efficiency. N_0 was determined to be 0.42 in a solution of 5 mM $K_4Fe(CN)_6$ + 0.5 mM $K_3Fe(CN)_6$.

Zn-air battery assembly: Briefly, 4 mg of catalysts and 10 μL of 5 wt. % Nafion solution were dispersed in 1 mL of ethanol by sonication. The obtained catalyst ink (Cu-BTA/C or 20% Pt/C) was cast onto carbon paper (Hesen, China) with a 1.5 cm diameter to form the air cathode. The catalyst loading was 991 μg cm^{-2}. A zinc foil and 6.0 M KOH solution containing 0.2 M $ZnCl_2$ were used as the anode and electrolyte, respectively. Polarization curves were recorded by linear sweep voltammetry (10 mV s^{-1}) on a CHI760E electrochemical platform to characterize the zinc-air battery performance. The galvanostatic discharge curves of the zinc-air batteries were recorded using an automatic battery testing system (LANHE CT2001A).

Equivalent diffusion coefficient (D_E) measurement: Given that O_2 enters the catalytic sites in a hydrated manner during the ORR, the effect of the different wettable catalytic surfaces on the O_2 diffusion abilities was evaluated using the equivalent diffusion coefficient (D_E) according to Equation (1):

$$I_D=0.4958nFAC \times D_E^{1/2} (n\alpha F/RT)^{1/2}\nu^{1/2} \quad (1)$$

where C was the O_2 concentration, T was temperature, n was the electron transfer number, α was the electron transfer coefficient, F and R were the Faraday constant and gas constant, respectively. A represents the electrochemically active area of the catalyst, which is proportional to C_{dl}.

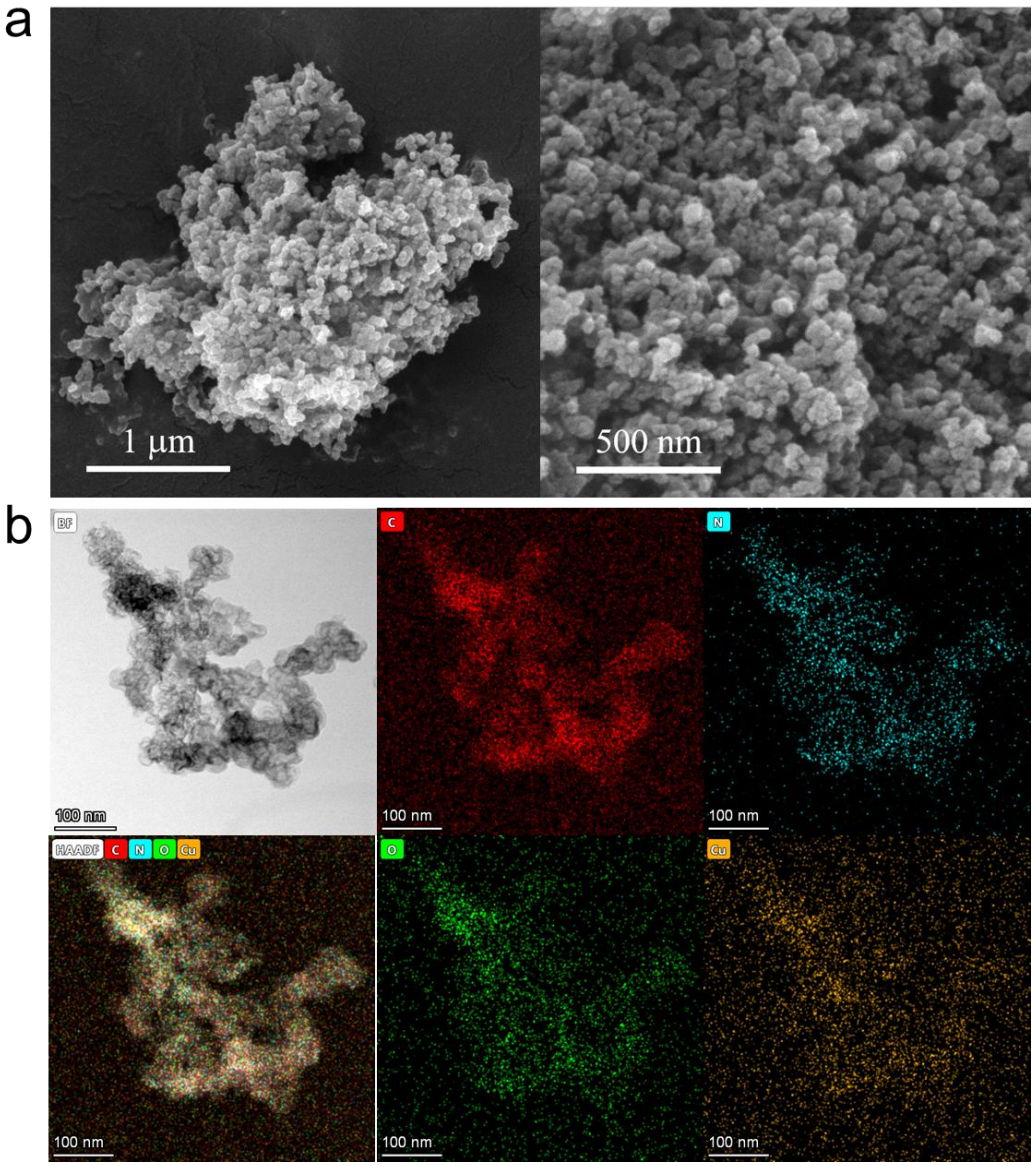

Figure S1 (a) SEM image of Cu-BTA/C. (b) TEM elemental mapping of Cu-BTA/C.

TEM images showed that Cu-BTA/C was agglomerated and mainly consisted of nanoparticles with sizes of ca. 20-30 nm (Figure S1). The corresponding TEM elemental mapping images in Figure S1b further verify that Cu-BTA is uniformly coated on the surface of CB. Therefore, by pre-absorbing conjugated BTA on CB as the ligand and backbone, Cu-BTA/C could be formed on the surface of CB with further complexation with Cu ions.

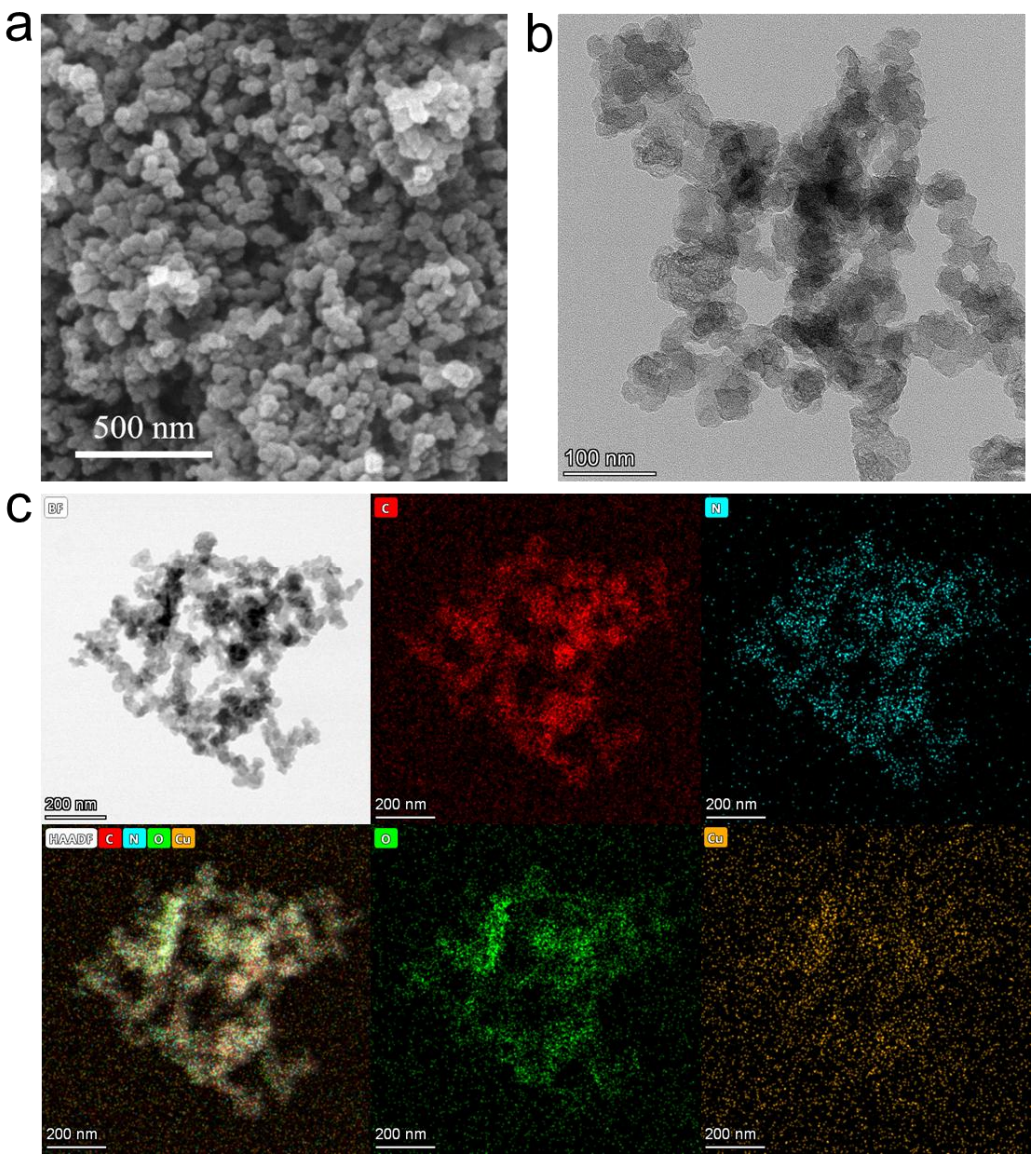

Figure S2 (a) SEM image of Cu-DAB/C. (b) TEM image of Cu-DAB/C. (c) TEM elemental mapping of Cu-DAB/C.

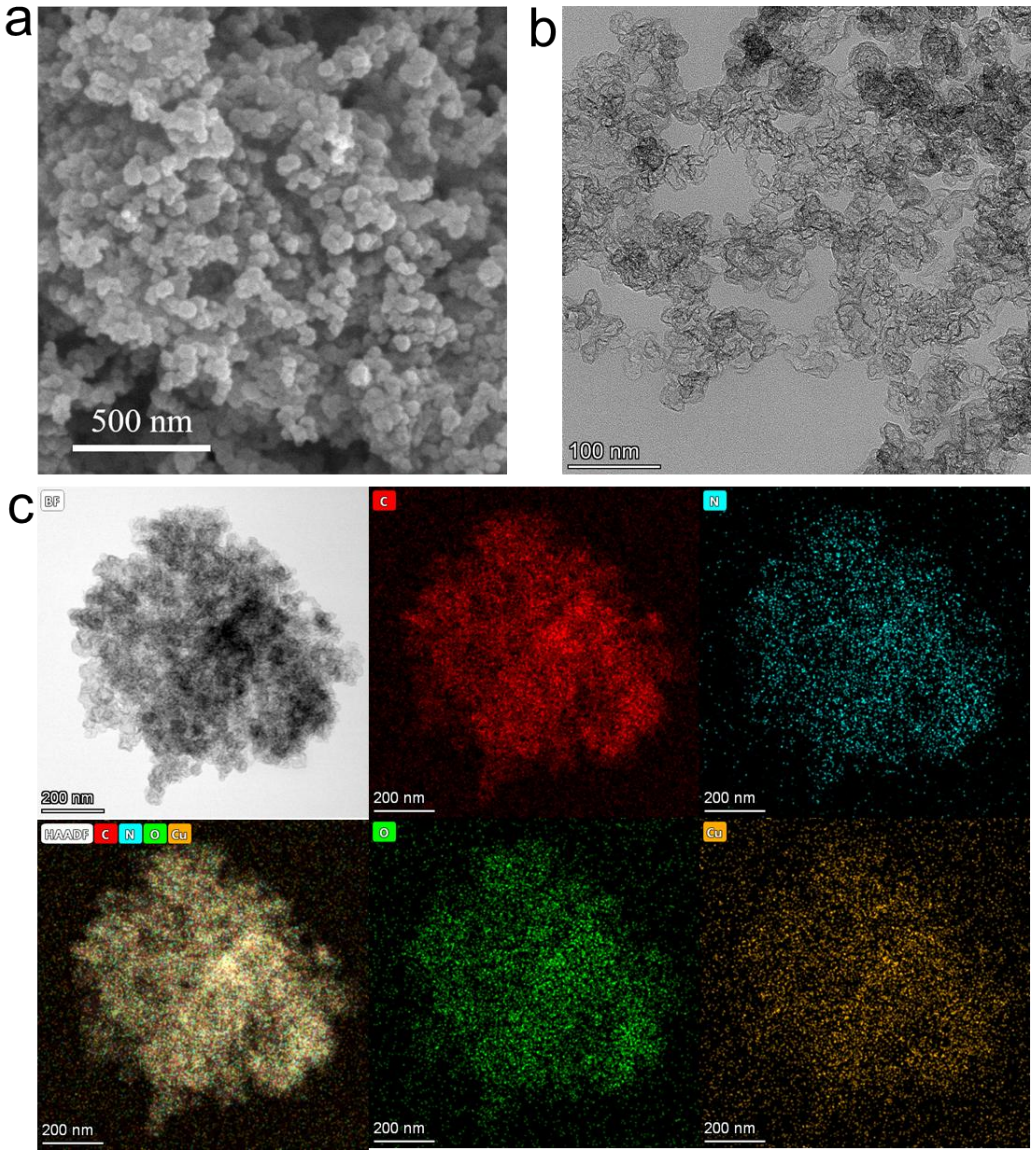

Figure S3 (a) SEM image of Cu-DAR/C. (b) TEM image of Cu-DAR/C. (c) TEM elemental mapping of Cu-DAR/C.

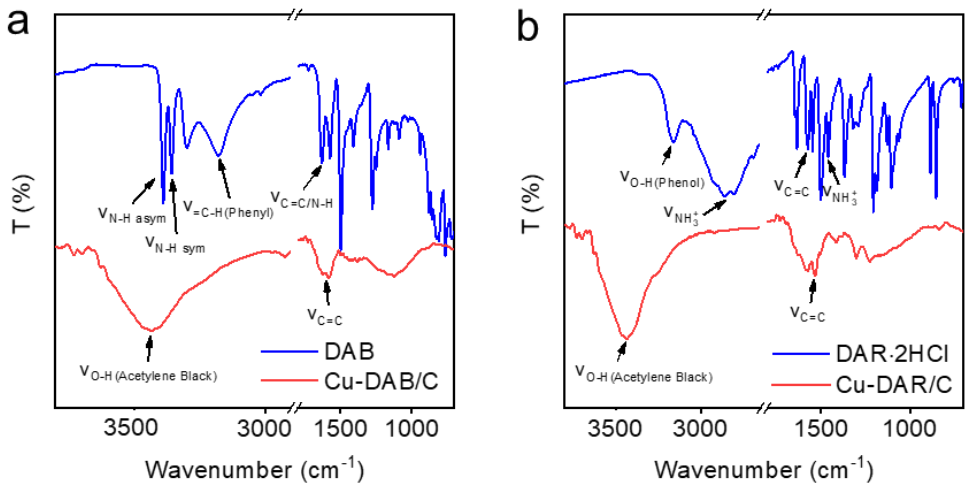

Figure S4 FT-IR spectra of (a) Cu-DAB/C and (b) Cu-DAR/C.

As shown in Figure S4a, the FT-IR spectra revealed that the characteristic $-NH_2$ groups ($\nu_{N-H\ asym/sym}$) of DAB at ca. 3389 cm^{-1} and 3356 cm^{-1} disappeared in Cu-DAB/C, whereas other phenyl-related vibrations remained, and a characteristic hydroxyl group (ν_{O-H}) belonging to CB appeared at ca. 3450 cm^{-1}. For Cu-DAR/C, the non-hydrochloride form of DAR is not available, and the characteristic $-NH_3^+$ groups of DAR·2HCl at ca. 2800-2900 cm^{-1} and the characteristic phenol groups at ca. 3160 cm^{-1} disappeared in Cu-DAR/C. These results demonstrate the coordination interaction between Cu and the ligands.

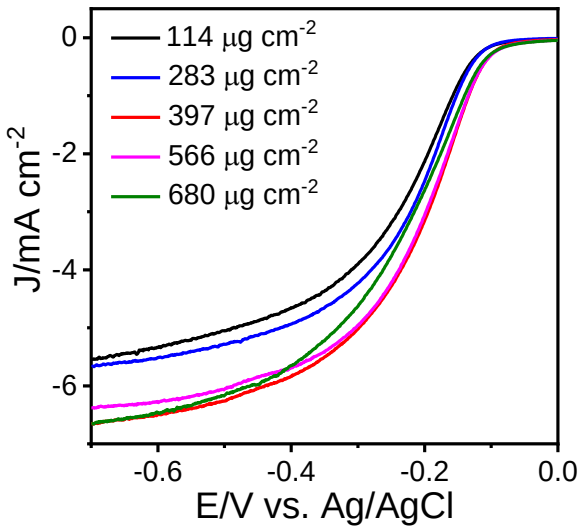

Figure S5 LSV curves of various loading amounts of Cu-BTA/C on electrode.

It indicates that Cu-BTA/C with a loading of 397 μg cm^{-2} on the electrode exhibited the best ORR performance.

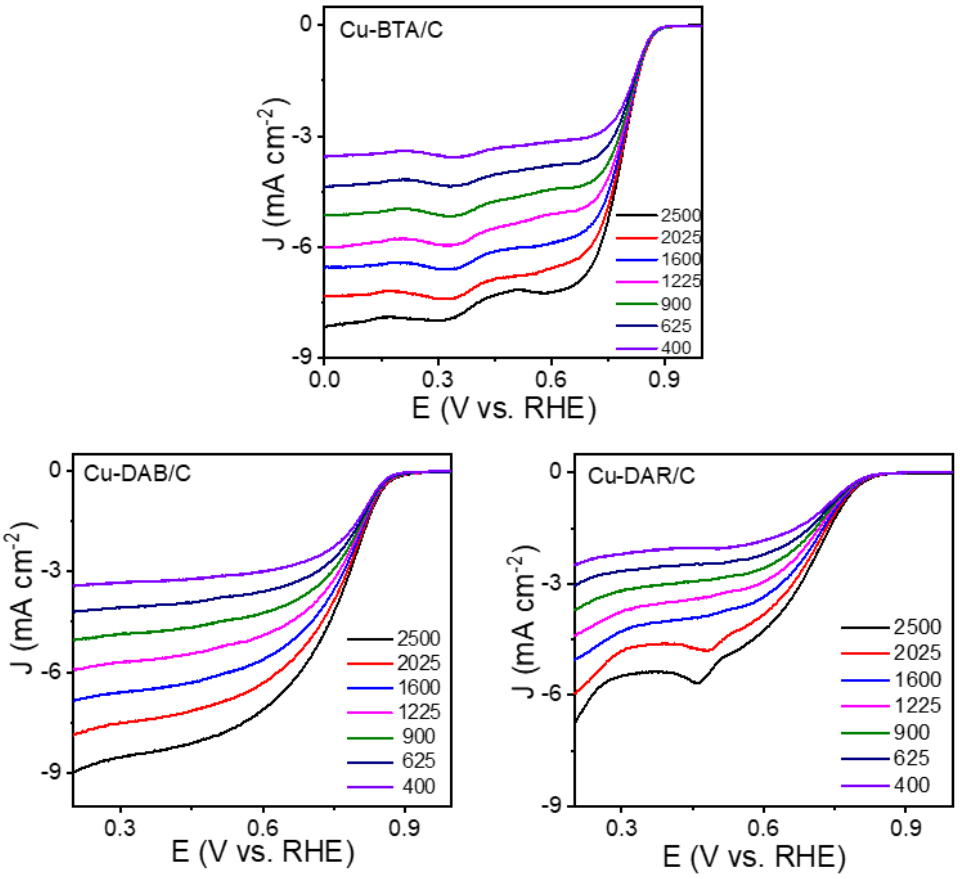

Figure S6 LSV curves of Cu-based catalysts with different rotation rates (revolutions per minute) in O_2-saturated 0.1 M KOH

All Cu-based catalysts exhibited a typical increase in current with higher rotation speeds (Figure S6), indicating that the ORR catalyzed by Cu-based catalysts was a diffusion-controlled process.

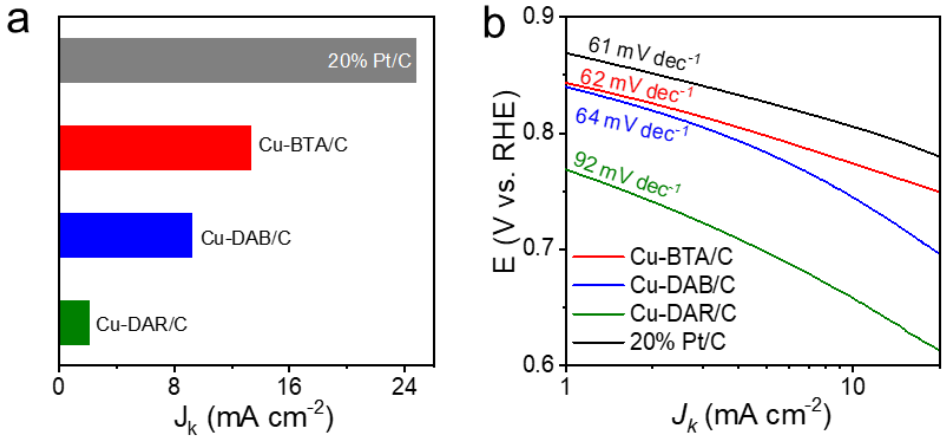

Figure S7 (a) J_k of various Cu-based catalysts and Pt/C at 0.75 V in O_2-saturated 0.1 M KOH solution. (b) Tafel plots of various Cu-based catalysts and Pt/C. Sweep rate: 10 mV s^{-1}.

The kinetic limiting current (J_k) of Cu-BTA/C was greater than that of Cu-DAB/C and Cu-DAR/C and approached that of commercial 20% Pt/C, indicating its excellent ORR performance. Figure S7b shows that the Tafel plot slope of Cu-BTA/C in the low overpotential region is close to 60 mV dec^{-1}, indicating that the first electron transfer is likely the rate-determining step in its catalytic ORR process, similar to Pt/C.

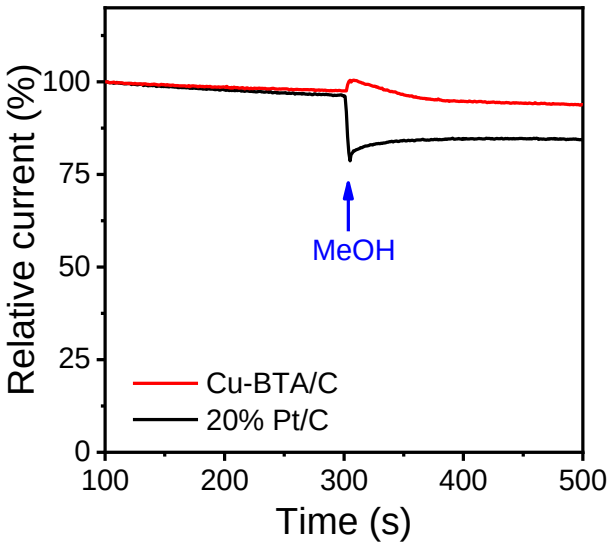

Figure S8 Crossover effect evaluation of methanol oxidation of Cu-BTA/C and 20% Pt/C.

Cu-BTA/C showed high stability and little crossover from methanol oxidation compared to Pt/C.

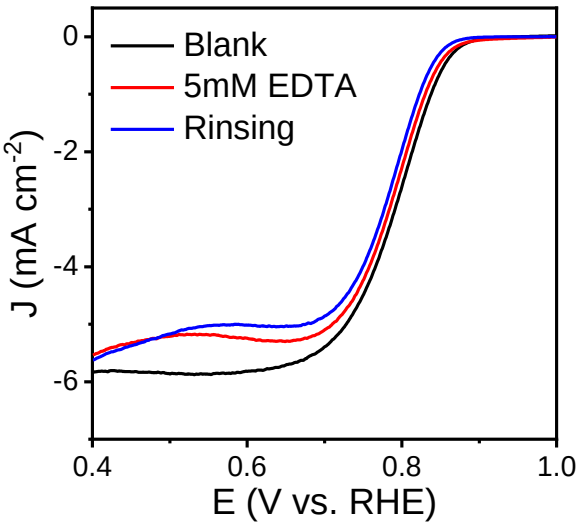

Figure S9 LSV curves of Cu-BTA/C in O_2-saturated 0.1 M KOH without EDTA, with 5 mM EDTA, and after EDTA poisoning tests, electrode rinsing, and immersion in O_2-saturated 0.1 M KOH.

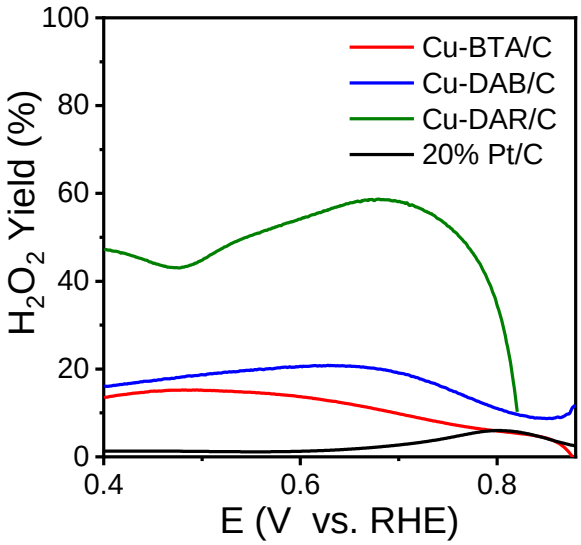

Figure S10 H_2O_2 yields of various Cu-based catalysts and Pt/C.

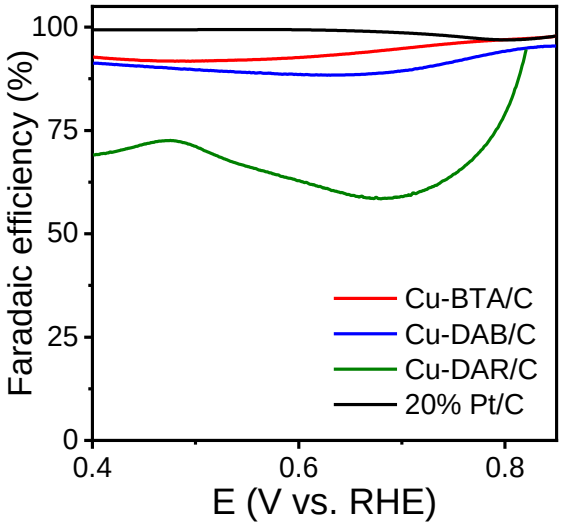

Figure S11 Faradaic efficiency of ORR catalyzed by various Cu-based catalysts and Pt/C.

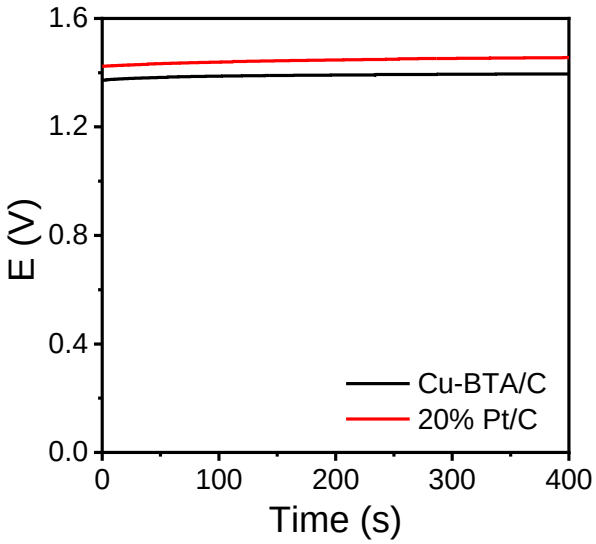

Figure S12 Open-circuit voltage curves of Zn-air battery with Cu-BTA/C and Pt/C cathodes.

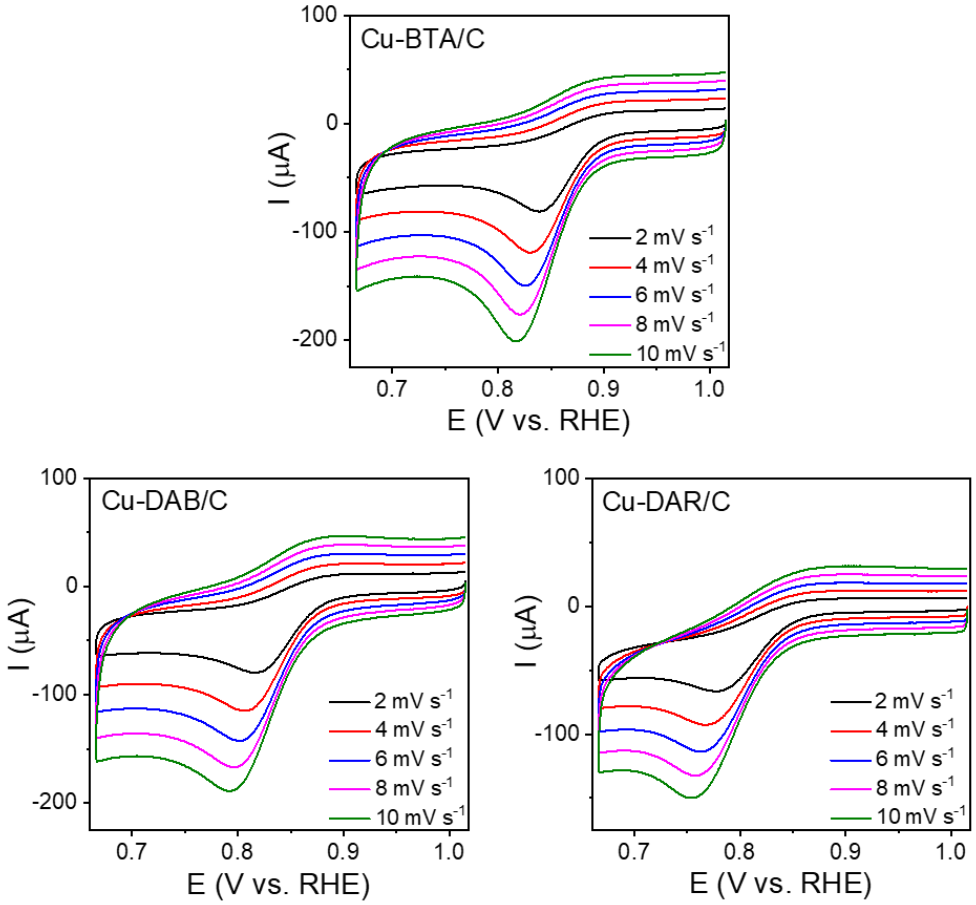

Figure S13 CV curves of various Cu-based catalysts in O_2-saturated 0.1 M KOH solution.

Table S1 Elemental analysis (EA) and inductively coupled plasma mass spectroscopy (ICP-MS) results for various Cu-based catalysts.

Weight ratio	Cu%	N%	C%	H%	L/Cu (Molar ratio)
Cu-BTA/C	10.84	10.94	77.14	1.08	1.14:1
Cu-DAB/C	8.22	8.21	79.42	4.16	1.14:1
Cu-DAR/C	9.52	5.74	80.59	4.15	1.37:1